Solutions for an efficient arsenite oxidation and removal from groundwater containing ferrous iron

Chaoyun Ying, Chang Liu, Feng Zhang, Lirong Zheng, Xiaoming Wang, Hui Yin, Wenfeng Tan, Xionghan Feng, Bruno Lanson

Solutions for an efficient arsenite oxidation and removal from groundwater containing ferrous iron

Chaoyun Ying[a,b,c], *Chang Liu*[a,b], *Feng Zhang*[a,b], *Lirong Zheng*[d], *Xiaoming Wang*[a,b], *Hui Yin*[a,b], *Wenfeng Tan*[a,b], *Xionghan Feng*[a,b*], *Bruno Lanson*[c]

[a] State Environmental Protection Key Laboratory of Soil Health and Green Remediation, Wuhan 430070, China.

[b] Key Laboratory of Arable Land Conservation (Middle and Lower Reaches of Yangtze River), Ministry of Agriculture, College of Resources and Environment, Huazhong Agricultural University, Wuhan 430070, China.

[c] Univ. Grenoble Alpes, CNRS, Univ. Savoie Mont Blanc, IRD, Univ. Gustave Eiffel, ISTerre, F-38000 Grenoble, France.

[d] Beijing Synchrotron Radiation Facility, Institute of High Energy Physics, Chinese Academy of Sciences, Beijing 100039, China.

*Corresponding author:
Xionghan Feng,
Tel: +86 27 87280271; Fax: +86 27 87288618; E-mail: fxh73@mail.hzau.edu.cn

Highlights:

- Fe(II) inhibits As(III) oxidation by aggravating birnessite surface passivation
- Pyrophosphate (PP) in reactive medium highly enhances As(III) oxidation
- PP prevents Mn oxide surfaces passivation, keeping As/Fe species in solution
- In the presence of Fe(II) and PP, generated ROS enhances As(III) oxidation further
- Removal of As(V) through sorption to Fe oxides is efficient in the presence of PP

Graphical Abstract

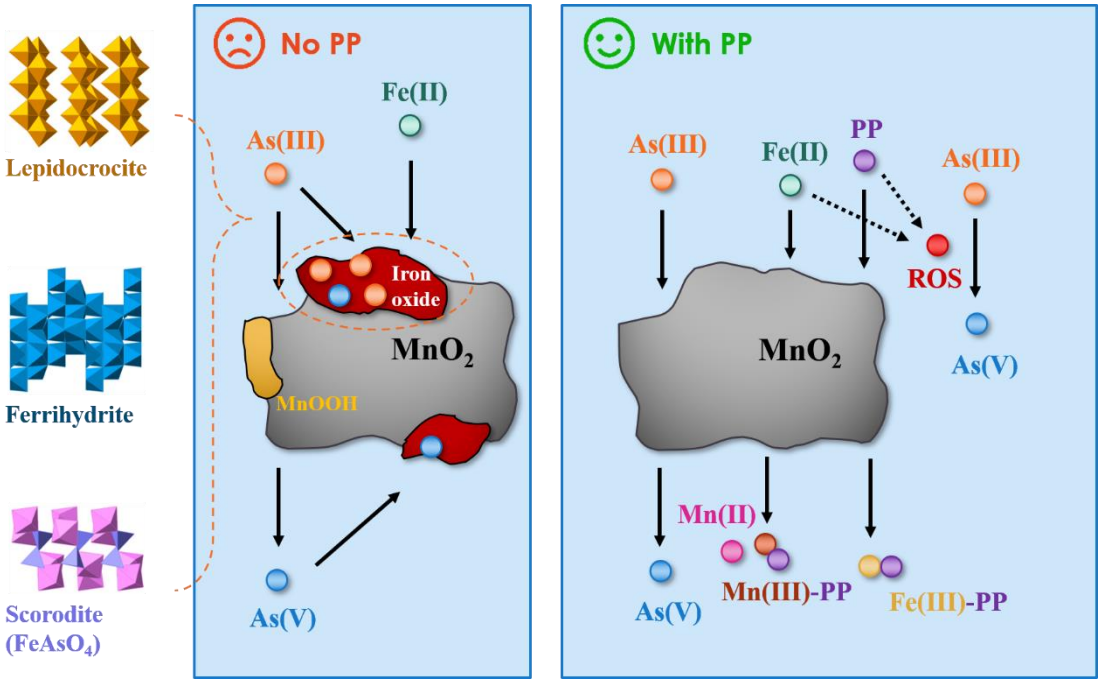

Abstract

Manganese (Mn) oxides are extensively used to oxidize As(III) present in ground, drinking, and waste waters to the less toxic and more easily removable As(V). The common presence of multiple other cations in natural waters, and more especially of redox-sensitive ones such as Fe^{2+}, may however significantly hamper As(III) oxidation and its subsequent removal. The present work investigates experimentally the influence of Mn(III) chelating agents on As(III) oxidation process in such environmentally relevant complex systems. Specifically, the influence of sodium pyrophosphate (PP), an efficient Mn(III) chelating agent, on As(III) oxidation by birnessite in the presence of Fe(II) was investigated using batch experiments at circum-neutral pH. In the absence of PP, competitive oxidation of Fe(II) and As(III) leads to Mn oxide surface passivation by Fe(III) and Mn(II/III) (oxyhydr)oxides, thus inhibiting As(III) oxidation. Addition of PP to the system highly enhances As(III) oxidation by birnessite even in the presence of Fe(II). PP presence prevents passivation of Mn oxide surfaces keeping As and Fe species in solution while lower valence Mn species are released to solution. In addition, reactive oxygen species (ROS), tentatively identified as hydroxyl radicals (•OH), are generated under aerobic conditions through oxygen activation by Fe(II)–PP complexes, enhancing As(III) oxidation further. The positive influence of Mn(III) chelating agents on As(III) oxidation most likely not only depend on their affinity for Mn(III) but also on their ability to promote formation of these active radical species. Finally, removal of As(V) through sorption to Fe (oxyhydr)oxides is efficient even in the presence of significant concentrations of PP, and addition of such Mn(III) chelating agents thus appears as an efficient way to enhance the oxidizing activity of birnessite in large-scale treatment for arsenic detoxification of groundwaters.

Keywords: *birnessite; arsenite oxidation; pyrophosphate; ferrous iron; reactive oxygen species; groundwater treatment*

1. Introduction

Arsenic (As) naturally occurring in groundwater affects millions of people worldwide (Chen et al., 2011; Frisbie and Mitchell, 2022; Podgorski and Berg, 2020; Razo et al., 2011; Smith and Steinmaus, 2011). Because of its high toxicity, the World Health Organization has set the maximum concentration for this element in drinking water to 10 µg/L (WHO, 2011). In natural environments, As is mainly present as inorganic species, arsenite [As(III)] and arsenate [As(V)] being predominant (Qin et al., 2016; Schaefer et al., 2020; Zheng et al., 2020). Arsenite is more toxic and mobile than arsenate in aqueous environments, and also more difficult to remove owing to its low affinity for sorbents (Zhang et al., 2018). Oxidizing As(III) into the more readily extractable As(V) thus appears as an efficient way to lower its toxicity and to achieve arsenic immobilization (Parikh et al., 2010; Wang et al., 2022; Zhu et al., 2009).

In this general context, manganese (Mn) oxides have been extensively used to oxidize As(III) (Gao et al., 2022; Oscarson et al., 1981; Villalobos et al., 2014). The common presence of multiple other cations in natural waters is however a critical factor that can influence oxidation and sorption of As(III). For example, the presence of calcium (Ca), the most frequent divalent cation in drinking water, decreases slightly As(III) oxidation rate (Driehaus et al., 1995). The presence of redox-sensitive cations is even more influential, with Mn(II) ion totally hindering As(III) oxidation by birnessite (Ehlert et al., 2014), because of Mn(II) and Mn(IV) comproportionation that leads to the formation of Mn (oxyhydr)oxides (Lefkowitz et al., 2013). The ubiquitous and naturally abundant ferrous ion [Fe(II)] also inhibits As(III) oxidation (Ehlert et al., 2014; Han et al., 2011; Huang et al., 2021). In this specific case, inhibition was attributed to the competitive oxidation of Fe(II) and As(III) (Ehlert et al., 2014; Gude et al., 2017; Mock et al., 2019) and to passivation of Mn oxide surfaces by Fe(III) precipitates following Fe(II) oxidation (Han et al., 2011; Mock et al., 2019; Zhang et al., 2020). These Fe(III) (oxyhydr)oxides provide adsorption sites for As and thus promote its removal from solution however (Gude et al., 2017; Han et al., 2011). Consistently, As is often associated with Fe oxides in soils and sediments and can be released by the reductive dissolution of its carrier phases (Herbel and Fendorf, 2006; Morin and Calas, 2006; Zhang et al., 2021). As a consequence, elevated concentrations of As(III) and Fe(II) are often coexisting in groundwater under moderately reducing conditions (He and Hering, 2009; Nickson et al., 2000; Wu et al., 2015).

The pH of groundwaters, especially when used as a source of drinking water, is mostly circumneutral (Camacho et al., 2011; Gunarathna et al., 2016; Hájek et al., 2020). To process such groundwaters, biogenic MnO_2 is often used as a coating on filtering sand grains to oxidize As(III) (Spiro et al., 2010), biotically mediated oxidation being an efficient alternative (Gude et al., 2017; Huang et al., 2023). In the former reaction, MnO_2 acts as an electron acceptor for As(III) but also for Fe(II), thus leading to the formation of hydrous ferric oxides (Gude et al., 2017; Sun et al., 2018) on its surface, these Fe (oxyhydr)oxides being inactive with respect to As(III) oxidation (Oscarson et al., 1981). Along the As oxidation process, formation of both Fe(III) and Mn(III) (oxyhydr)oxides steadily passivates the surface of the initial MnO_2 (Ehlert et al., 2014; Gude et al., 2017; Lefkowitz et al., 2013), thus reducing its oxidizing activity. Addition of pyrophosphate (PP), an efficient Mn(III) chelating agent (Jung et al., 2017; Liu et al., 2019; Qian et al., 2019), to the system allows inhibiting the precipitation of solid Mn(III) (oxyhydr)oxides and thus enhances As(III) oxidation by birnessite at circum-neutral pH (Ying et al., 2020). Additional complexity induced by the presence of Fe(II) in the As(III)-MnO_2-PP system has been little investigated however and essentially no information is available in the literature on As(III) oxidation in such realistic systems.

The present work thus aims at investigating experimentally the influence of PP on As(III) oxidation by birnessite in the As(III)-MnO_2-PP-Fe(II) system using a combination of wet chemical analyses and crystal-chemical characterization. As in previous studies on this topic (Lan et al., 2018; Ying et al., 2020), PP was selected as a model Mn(III) chelating agent due to its representative binding affinity (Nico and Zasoski, 2001; Wang et al., 2014), redox-inertness (Wang et al., 2020), and wide occurrence in natural (Klewicki and Morgan, 1999; Trouwborst et al., 2006) and engineered aquatic systems (Sun et al., 2015). The efficiency of subsequent As removal treatment was also assessed using two-line ferrihydrite (2L-Fh) which is known as an efficient As(V) adsorbent (Raven et al., 1998).

2. Materials and Methods

2.1 Chemicals

All chemicals used in the present study were purchased from Sinopharm Chemical

Reagent, except for leucoberbelin blue I (Sigma Chemical Company), potassium borohydride (Lingfeng Chemical Reagent Co., LTD), formic acid (Fisher Chemical), and 5,5-Dimethyl-1-pyrroline N-oxide (DMPO, 97% – Shanghai Aladdin Bio-Chem Technology Co., LTD). Atomic absorption spectroscopy Mn and Fe standards were prepared from the dilution of 1000 mg/L commercial standards. Deionized water (18.2 MΩ·cm) was used in all experiments.

2.2 Synthesis of Hexagonal Birnessite and Two-line Ferrihydrite

Synthetic hexagonal birnessite was prepared by the dropwise addition of 45 mL of a 6 M HCl solution to 300 mL of a boiling 0.667 M solution of $KMnO_4$ (McKenzie, 1971; Ying et al., 2020). The obtained suspension was stored at 60 °C for 12 h to increase birnessite crystallinity. The resulting solid was then washed with deionized water to remove K^+ and Cl^- in excess (Ying et al., 2020).

Two-line ferrihydrite (2L-Fh) was synthesized by adding under stirring a 2 M NaOH solution to a 500 mL solution containing 40 g $Fe(NO_3)_3 \cdot 9H_2O$, until the pH reached 7-8 (Zhang et al., 2022). After 2 h of equilibration time, the suspension was washed with deionized water and centrifuged (5×) to remove Na^+ and NO_3^- in excess. The obtained 2L-Fh suspension was then stored at 4 °C. The concentration of the 2L-Fh suspension was determined by weighing after evaporation the dry solid contained in 2 mL of suspension (measurement was duplicated).

2.3 As(III) Oxidation Batch Experiments and Wet Chemical Analyses

Batch experiments were conducted at room temperature in 100 mL conical flasks open to the atmosphere. 100 mL of a 0.2 g/L birnessite suspension were equilibrated at pH 7 in a 0.1 M NaCl background electrolyte before 0.5 mM As(III) were introduced together with and 0, 0.10, 0.25, and 0.50 mM Fe(II) (introduced as $FeSO_4 \cdot 7H_2O$). pH was monitored and adjusted along the experiments using a potentiometric titrator (Metrohm 907). Aliquots (2 mL) were collected from the suspension at pre-determined time intervals and readily syringe-filtered using 0.22-µm nitrocellulose membranes. Similar batch experiments were performed in the presence of 0.5, 2.5, and 5.0 mM sodium pyrophosphate (PP), with manual pH adjustment however, using 0.5 mM HCl/NaOH solutions. Experimental conditions and key parameters are listed in Table 1. After 24 h reaction time, solid products were filtered, washed thoroughly with

deionized water to remove residual dissolved ions and freeze-dried. Additional experiments were performed under anoxic conditions in a Longyue anaerobic chamber in the presence of 0 and 5.0 mM PP, respectively. In this case, deionized water was boiled and degassed prior to the preparation of the solutions.

Total Fe and Mn concentrations in solution were determined using atomic absorption spectrometry (AAS – Agilent Technologies 200 series). Mn(III) aqueous concentration was determined colorimetrically using leucoberbelin blue dye and absorption at 620 nm (Zhu et al., 2017). Mn species present in solution were identified from their spectroscopic signature in the UV-visible range (Agilent Technologies Cary 8454). In the experiments without PP, As(V) and total As concentrations were determined using the ammonium molybdenum method (Feng et al., 2018), the concentration of As(III) concentration being calculated as the difference between total As and As(V). In the presence of PP, As(III) and As(V) were determined using coupled liquid chromatography – atomic fluorescence spectrophotometer (LC-AFS, Kylin S12, Beijing Jitian Instruments Co Ltd), As(III) and As(V) being separated by liquid chromatography (Hamilton PRP-X100) using 15 mM diammonium hydrogen phosphate solution, whose pH value was adjusted to 6.0 using 10% formic acid, at 1 mL/min flow rate. The outflow from the LC was directly connected to the AFS for As quantification.

2.4 Electron Paramagnetic Resonance Detection of Radical Species

Reactive oxygen radicals formed during the reactions between Fe(II) and PP were identified using electron paramagnetic resonance (EPR). Solution samples were analyzed on a Bruker EMXnano spectrometer using 5, 5-dimethyl-l-pyrroline-N-oxide (DMPO) as radical trapper (Wang et al., 2013; Wu et al., 2020).

2.5 As(V) Adsorption Experiment

To assess the influence of PP added in the As(III) oxidation experiments on the subsequent removal of As(V) from solution, 0.5 mM of As(V) were added to 100 mL of a 5 g/L 2L-Fh suspension (0.1 M NaCl background electrolyte) that also contains 2.5 mM PP. pH was manually adjusted along the experiments with 0.5 M HCl. Aliquots (2 mL) were collected from the suspension at pre-determined time intervals and readily syringe-filtered using 0.22-μm nitrocellulose membranes. Total As, P, and Fe

concentrations in solution were determined using inductively coupled plasma-optical emission spectrometer (ICP-OES, Varian 720-ES).

2.6 Solid Product Characterization

X-ray powder diffraction (XRD). Synthetic birnessite and ferrihydrite and all solid reaction products were characterized by XRD using a Bruker D8 Advance diffractometer equipped with a LynxEye detector and Ni-filtered Cu Kα radiation (λ = 0.15418 nm). The diffractometer was operated at 40 kV and 40 mA, data being collected at a scanning rate of 4°/min with 0.02° steps.

Field-emission scanning electron microscopy (FESEM) and energy-dispersive X-ray fluorescence spectroscopy (EDS). Gold-coated samples were observed using FESEM with a maximum resolution of 1 nm, when coupled with EDS mapping (S4800, Hitachi Limited, Japan). For high-resolution images, the microscope was operated at 10 kV using a working distance of 10-15 mm, and an in-lens secondary electron detector.

Fe/As K-edge X-ray absorption near edge structure (XANES) spectroscopy and Fe/As speciation analysis. XANES spectra were collected at room temperature on the 1W1B beamline of the Beijing Synchrotron Radiation Facility. Data was collected in fluorescence mode over the 6.9-7.8 keV and 11.7-12.6 keV ranges (Fe and As K-edges, respectively). Energy calibration was systematically performed before data collection using Fe or As metal foil. Fe K-edge spectra were averaged and background-subtracted using the following parameters: E_0 = 7127.61 eV, Rbkg = 1 Å, and k-weight = 2. Arsenic K-edge spectra were averaged and background-subtracted using the following parameters: E_0 = 11875.5 eV, Rbkg = 1 Å and k-weight = 2. The Athena program was used for background removal and linear combination fits (LCF) to assess Fe and As speciation (Ravel and Newville, 2005).

Lepidocrocite, ferrihydrite, and scorodite ($FeAsO_4$) were used as Fe reference standards. The three Fe standards were prepared as described in Liao et al. (2020), Lan et al. (2017), and Mikutta et al. (2014), respectively. As(III) and As(V) sorbed to ferrihydrite were used as standards to quantify As oxidation state. These standards were prepared by adding 0.4 mM As(III/V) to 1 L of a 1 g/L ferrihydrite suspension. After stirring for one hour, the resulting As(III/V) sorbed ferrihydrite suspension was filtered, washed thoroughly with deionized water to remove residual dissolved ions, air-dried,

and ground.

Fourier transform infrared (FTIR) spectroscopy. FTIR spectra were collected in transmission mode using a Bruker Vertex 70 spectrometer equipped with a deuterated triglycine sulfate detector (Bruker Optics Inc.). Thirty-two scans were collected over the 4000-400 cm^{-1} range (4 cm^{-1} resolution) and averaged for each sample, data being collected, processed, and analyzed with the OPUS program.

3 Results and discussion

3.1 As(III) Oxidation by Birnessite in the Presence of Fe(II) with/without PP

At pH 7 and after 24 h of reaction in the absence of Fe(II) in the system, 60% of As(III) initially present in solution is oxidized to As(V) by birnessite. Additional presence of Fe(II) in the system decreases the extent of As(III) oxidation in solution with 49, 22, and 11% of As(III) initially present in solution oxidized to As(V) after 24 h (Fig. 1a-e – 0.5, 2.5, and 5.0 mM Fe(II), respectively). The lower concentrations of As(V) measured in solution after 24 h in the presence of Fe(II) result both from the decreased efficiency of As(III) oxidation (Fig. 1e) and from increased As removal from solution, most likely as the result of sorption on birnessite and/or on newly formed Fe (oxyhdr)oxides. Sorption of As on birnessite appears limited however, as 94% of the As initially introduced remains in solution after 24 h in the absence of Fe(II) (Fig. 1a). On the other hand, Fe is readily removed from solution with essentially no Fe being detected in solution after a few minutes (Fig. 1f), most likely as the result of Fe(II) oxidation and precipitation as Fe(III) (oxyhydr)oxides at the birnessite surface. Owing to their higher adsorption affinity for As compared to birnessite (Ying et al., 2012), these newly formed Fe(III) (oxyhydr)oxides most likely serve as sorbent for As (Ehlert et al., 2014). Formation of Fe(III) (oxyhydr)oxides on birnessite surface likely passivates this surface as reported for the formation of Mn (oxyhydr)oxides (Gude et al., 2017; Ying et al., 2020), consistent with the limited efficiency of As(III) oxidation in the presence of Fe(II) (Fig. 1a-e). Presence of Fe(II) in the system does not appear to influence significantly Mn release to solution that remains limited in all cases (Fig. 1g).

As reported previously for Fe-free systems (Ying et al., 2020), As(III) oxidation is dramatically enhanced in the presence of PP and 0.5 mM Fe(II), as essentially all As(III)

initially present in solution is oxidized by birnessite in the presence of 5 mM PP, a tenfold increase compared to the PP-free system (Figs. 1d, 2a-d). PP addition prevents indeed precipitation of both Fe and Mn (oxyhydr)oxides at the birnessite surface (Fig. 2e, f), thus avoiding its passivation (Ying et al., 2020) and favoring As(III) oxidation (Fig. 2a-d). Consistently, increased intensity of the absorption band at 258 nm upon As(III) oxidation [Fig. S1a – Ying et al. (2020)] and the Mn(III) concentrations determined with the LBB method revealed the presence of Mn(III)-PP complexes in solution (Fig. 2f). A control experiment performed in the absence of birnessite shows that Fe-PP complexes do not generate absorption in the probed UV-Vis range and thus allows ruling out a possible bias induced by the presence of aqueous Fe species (Fig. S1b). Contrasting with other organic ligands such as oxalate (Ying et al., 2020) or citrate (Liang et al., 2020), and consistent with preliminary data (not shown), the reaction between the pyrophosphate, which is considered to be a nonredox active ligand (Morgan et al., 2021), and birnessite could be disregarded.

As(V) formation kinetics in solution can be approximated using a pseudo-second order model. The pseudo-second-order kinetic equation is as follows (Pan et al., 2010):

$$C_t = \frac{C_e^2 kt}{1 + C_e kt}$$

in which C_t is the As(V) concentration in solution at time t, C_e is the equilibrium As(V) concentration in solution and k (h^{-1}) is As(V) formation rate constant.

Fig. S2a shows that during the As(III) oxidation by birnessite, the value of the rate constant k sharply decrease from 4.24 (k_1) to 9.5×10^{-8} (k_4) when increasing the initial Fe(II) concentration from 0 mM to 0.5 mM; When k is large, the $C_t = f(t)$ curve rises steeply to the equilibrium state. On the contrary, a low value of C_t causes the curve to approach its equilibrium much more slowly. Finally, the presence of PP in the system enhances As(III) oxidation to As(V) with up to ~100% of As(III) initially introduced being oxidized, but increases the time necessary to reach equilibrium (Fig. S2b).

3.2 Identification of the Solid Products

When reacting with As(III) in the absence of PP, birnessite nano-flowers (Fig. 3a) are "filled" after 24 h of reaction, nano-flake edges becoming blurred (Fig. 3b), owing to Mn(III) precipitates formed at the birnessite surface from Mn(II) and Mn(IV) comproportionation (Ying et al., 2020). The additional presence of Fe(II) in the system

leads to the additional formation of Fe- and As-rich precipitates at the birnessite surface (Figs. 3c, S3a, Table S1). By contrast, the presence of PP in solution allows birnessite surface to keep its original appearance during As(III) oxidation process (Fig. 3d), consistent with previous report on Fe-free experiments (Ying et al., 2020), and to remain free of Fe and As precipitates (Fig. S3b, Table S1), consistent with constant Fe and As concentrations measured in solution in the presence of PP (Fig. 2c-e).

Reflections at 0.723, 0.361, 0.244, and 0.142 nm typical for turbostratic birnessite (Drits et al., 2007) are visible on birnessite XRD patterns both before and after reaction with As(III) in the presence of Fe(II) independent of the presence of PP (Fig. S4). In the presence of Fe(II) and absence of PP (Exp. Fe0.00_PP0.0 - Exp. Fe0.50_PP0.0), no characteristic peaks of Fe oxides are observed in the XRD patterns, suggesting the formation of poorly crystalline Fe/As precipitates difficult to detect using XRD. An increasing amount of these precipitates with increasing Fe content increases however X-ray absorption and thus decreases birnessite peak intensity (Fig. S4). Contrastingly, addition of PP to the system prevents the formation of these precipitates, thus leaving birnessite peak intensity unaffected compared to the initial birnessite (Fig. S4, Exp. Fe0.50_PP0.0 - Fe0.50_PP5.0). Manganite, that was reported in similar experiments performed in the absence of PP and Fe(II) (Ying et al., 2020), was not detected in the present study (Fig. S4). It should be noted however that in our previous experiments the presence of these precipitates was detected only when using synchrotron-based XRD (Ying et al., 2020), the precipitates remaining undetected with laboratory instruments used in the present study.

XANES spectroscopy performed at the Fe K edge helps exploring further the crystal chemistry of the mixed Fe/As precipitates formed at the birnessite surface (Fig. S5a, b). In all cases, the precipitate spectral signature is satisfactorily fitted using reference spectra of lepidocrocite, ferrihydrite, and amorphous $FeAsO_4$ (Fig. S5c, d). In the presence of 0.25 mM Fe(II), the precipitated Fe(II) on the surface of birnessite is most lepidocrocite (67%), and then amorphous $FeAsO_4$ (21%) and ferrihydrite (12%) after 24 h (Fig. S5c). When 0.5 mM Fe(II) is present, the contribution of lepidocrocite decreases to 55%, and then amorphous $FeAsO_4$ (23%) and ferrihydrite (22% – Fig. S5d). The increase in the concentration of ferrous ions does not change the proportion of amorphous $FeAsO_4$, but favors Fe precipitation as ferrihydrite.

In addition, FTIR spectra collected on the solid reaction products show the presence of As sorbed to these Fe (oxyhydr)oxides from the presence of additional

maxima over the 780-880 cm^{-1} range, compared to initial birnessite. Specifically, peaks at 782 cm^{-1}, at 825 and 876 cm^{-1} (Fig. 4a) may be attributed to As(III) and As(V) sorbed to Fe (oxyhydr)oxides (Bhandari et al., 2011; Cerkez et al., 2015), and their overall intensity appears to increase when increasing the amount of Fe(II) introduced in PP-free systems. Using As(III) and As(V) sorbed to ferrihydrite as references, XANES spectra collected at the As K-edge XANES consistently indicates that As sorbed to Fe (oxyhydr)oxides is present both as As(III) and As(V) (Fig. 4b). When increasing the initial amount of Fe(II) in the system, the relative proportion of sorbed As(III) increases from 28 (Exp. Fe0.25_PP0.0) to 50% (Fe0.50_PP0.0 – Fig. S6). The increasing amount of sorbed As(III) is possibly related to the increased proportion of ferrihydrite passivating birnessite surface (Ehlert et al., 2014). Consistently, higher initial Fe(II) concentrations in the solution enhance the formation of Fe (oxyhydr)oxides and As removal from solution (Fig. 1e) owing to the strong affinity of As for these mineral species (Gustafsson and Antelo, 2022; Lan et al., 2018; Raven et al., 1998; Ying et al., 2012).

3.3 The Underlying Reaction Mechanisms

In Exp. Fe0.00_PP0.0, 60% of As(III) introduced is oxidized to As(V), most of As (94%) remaining in solution, consistent with our previous work (Ying et al., 2020). Increasing the amount of Fe(II) in PP-free system results both in the overall decrease of As(III) oxidation efficiency and in the increase of As associated with the solid phase, as shown by the ratios of As species calculated from the relative proportions of As in aqueous and solid forms (Fig. 5). Compared to the Fe-free experiment the overall content of As(III) after 24 h reaction time increases indeed from 34% to 61 and 66% in Exp. Fe0.25_PP0.0 and Fe0.50_PP0.0, respectively (Fig. 5a). Simultaneously, the proportion of As associated to solid phases increases from 6% in the absence of Fe (Exp. Fe0.00_PP0.0) to 24 and 47%, respectively in Exp. Fe0.25_PP0.0 and Fe0.50_PP0.0 (Fig. 5b). Likely mechanisms for the As(III) oxidation by birnessite in the presence of Fe(II) may be deduced from the present results. First, As(III) and Fe(II) compete for the birnessite surface active sites and are both swiftly oxidized to As(V) and Fe(III), respectively (Eq. 1) (Wu et al., 2018). Part of Mn(II) released along this redox reaction is subsequently adsorbed to and oxidized by birnessite forming manganite (γ-MnOOH) (Eq. 2) (Ying et al., 2020) as described by Eqs. 1, 2:

$Fe(II) + As(III) + 2\ MnO_2 \rightarrow Fe(III) + As(V) + 2\ Mn(II)$ (Eq. 1)

$Mn(II) + MnO_2 + 2\ H_2O \rightarrow 2\ MnOOH + 2\ H^+$ (Eq. 2)

Fe(III) also precipitates at pH 7 to form poorly crystalline ferrihydrite and lepidocrocite (Fig. S5, Eq. 3) at the birnessite surface, leading to surface passivation and to the reduction of both As(III) and Fe(II) oxidation rates (Wu et al., 2018).

$Fe(III) + 2\ H_2O \rightarrow FeOOH\ (s) + 3\ H^+$ (Eq. 3)

In contrast to manganite, newly formed Fe(III) precipitates react with As to generate amorphous $FeAsO_4$ and As-rich ferrihydrite (Figs. 4, S5), contributing significantly to As sequestration in the solid fraction. For example, results reported in Fig. 5 for an initial Fe(II) concentration of 0.5 mM and in the absence of PP may be described by the following equation (Eq. 4):

$Fe^{2+} + 0.34\ AsO_3^{3-} + 1.68\ MnO_2 + 2.34\ H_2O \rightarrow$

$FeOOH\ (s) + 0.1\ AsO_4^{3-}{}_{aq} + 0.24\ AsO_4^{3-}{}_{sorbed/prec.} + 1.68\ MnOOH\ (s) + 2\ H^+$ (Eq. 4)

Consistent with previous reports (Ying et al., 2020), the addition of PP to the experiments allows keeping most As in solution with 88 and 100% of As present as aqueous species in Exp. Fe0.50_PP2.5 and Fe0.50_PP5.0, compared to 53% in the absence of PP (Exp. Fe0.50_PP0.0 – Fig. 5b). At the same time, As(III) oxidation is highly promoted with ~75% and 100% of initial As(III) being oxidized with the presence of 2.5 mM PP and 5.0 mM PP in solution, respectively, compared to 34% in the absence of PP (Exp. Fe0.50_PP0.0 – Fig. 5a).

In the absence of Fe, similar tendencies are observed that result from the strong chelating affinity of PP for Mn(III), thus preventing Mn(III) (oxyhydr)oxide precipitation at the birnessite surface (Ying et al., 2020). In the present experiments and in the absence of PP, birnessite surface passivation is aggravated by the presence of Fe(II), as both Mn(III) and Fe(III) (oxyhydr)oxides readily form at the birnessite surface (Figs. 1f, S3a, 3) (Ehlert et al., 2014; Gude et al., 2017). As reported previously (Ying et al., 2020), birnessite surface passivation hampers As(III) oxidation, this negative effect being associated to As sorption to the newly formed Fe (oxyhydr)oxides (Ehlert et al., 2014). Contrastingly, addition of PP to the system prevents the precipitation of both Fe(III) and Mn(III) (oxyhydr)oxides, thus favoring As(III) oxidation and keeping oxidized As species in solution (Fig. 5b). Accordingly, results reported in Fig. 5 for an initial Fe(II) concentration of 0.5 mM in the presence of 5.0 mM PP may be described by the following equation (Eq. 5 – x+y+z = 10):

$Fe^{2+} + AsO_3^{3-} + 2.08\ MnO_2 + 10\ PP + 0.14\ O_2 + 6.88\ H^+ \rightarrow$

369 $Fe(III)\text{-}xPP + AsO_4^{3-}{}_{aq} + 0.36\ Mn(II)\text{-}yPP + 1.72\ Mn(III)\text{-}zPP + 3.44\ H_2O$ (Eq. 5)

370 As reported in Eq. 5, O_2 is involved in the above-described oxic experiments. To
371 assess the influence of O_2, Exp. Fe0.50_PP0.0 and Fe0.50_PP5.0 were repeated under
372 anoxic conditions. In the anoxic Exp. Fe0.50_PP0.0_Anox, 35% of As(III) introduced
373 initially remains in solution (Fig. 6a), an amount similar to the 42% measured in the
374 equivalent oxic experiment (Fig. 1d). The overall amount of introduced As remaining
375 in solution after 24 h is also alike in the two experiments at 49 and 53% in anoxic and
376 oxic experiments, respectively (Figs. 6a, 1d). The overall decrease of As concentration
377 in solution is likely induced by As sorption on newly formed Fe (oxyhdr)oxides, the Fe
378 content in solution decreasing sharply at the beginning of the reaction (Fig. 6b), as
379 observed under oxic conditions and in the absence of PP (Fig. 1f). Consistent with oxic
380 experiments, addition of PP to the system allows preventing the precipitation of Fe
381 (oxyhdr)oxides, all Fe introduced remaining in solution (Fig. 6b). In addition, Mn
382 release to solution is significantly enhanced compared to the PP-free system (Fig. 6c),
383 being twofold that measured in the equivalent oxic Exp. Fe0.50_PP5.0 (Figs. 6c, 2f).
384 As a consequence, As(III) oxidation is enhanced by the presence of PP even in anoxic
385 conditions with up to 79% of As(III) introduced being present as As(V) in solution after
386 24 h, compared to 13% in the anoxic PP-free system (Fig. 6a). The large Fe and Mn
387 contents present in solution are consistent with the absence of birnessite surface
388 passivation but the amount of As(V) in solution is reduced by 24% compared to the
389 equivalent oxic Exp. Fe0.50_PP5.0 (from 0.51 to 0.39 mM – Figs. 2c, 6a). Although
390 Mn (oxyhydr)oxides are responsible for ~80% of As(III) oxidation, results from anoxic
391 experiments suggest the frequently overlooked ability of oxygen to oxidize As(III)
392 within 24 h (Feng et al., 2018; Lafferty et al., 2010; Parikh et al., 2010), especially when
393 Fe(II) and PP are present in the system.

394 The ability of Fe(II)-PP complexes to oxidize As(III) in the absence of birnessite
395 was assessed as a possible alternative to oxygen to account for the enhanced As(III)
396 oxidation observed under oxic conditions (Exp. Fe0.50_PP5.0_NoBirnAs). In this
397 experiment, ~0.1 mM As(III) is oxidized in the sole presence of PP and Fe(II) (Fig.
398 S7a). The seven peaks with the intensity ratio of 1:2:1:2:1:2:1 (Fig. S7b) present in the
399 experimental EPR spectra of a solution initially devoid of As(III) (Exp.
400 Fe0.50_PP5.0_NoBirnNoAs) are likely indicative of 5, 5-dimethylpyrroline-(2)-oxy-
401 (1) [DMPOX – Wu et al. (2020)], possibly resulting from DMPO interaction with •OH
402 radicals (Khachatryan and Dellinger, 2011). In the presence of As(III), these radicals

species are consumed by the oxidation of As(III) introduced in the system (Fig. S7b). The observed As(III) oxidation in the sole presence of PP and Fe is consistent with the observed enhancement of the Fe^{2+}/O_2 oxidizing ability resulting from the coexistence of Fe(II, III) with strong ligands such as tetrapolyphosphate [TPP – Wang et al. (2013)] or ethylenediaminetetraacetic acid [EDTA – Welch et al. (2002)]. Wang et al. (2013) attributed this enhancement to the production of $\bullet O_2^-$ and •OH radical species from the activation of oxygen and Fenton reactions [Eqs. 6-8 – Wang et al. (2013)]. A similar process may account for the formation of hydroxyl radicals (•OH) and for the induced enhancement of As(III) oxidation observed in the present experiments performed under oxic conditions and in the absence of birnessite.

$$Fe^{2+} + O_2 \rightarrow Fe^{3+} + \cdot O_2^- \quad \text{(Eq. 6)}$$

$$Fe^{2+} + \cdot O_2^- + 2\ H^+ \rightarrow Fe^{3+} + H_2O_2 \quad \text{(Eq. 7)}$$

$$Fe^{2+} + H_2O_2 \rightarrow Fe^{3+} + 2\ OH^- + \cdot OH \quad \text{(Eq. 8)}$$

3.4 Removal of As(V) from Solution through Sorption to Ferrihydrite in the Absence/Presence of PP

In the above-described series of experiments, addition of PP dramatically enhances As(III) oxidation by birnessite, even in the presence of competing redox-sensitive Fe(II), by preventing birnessite surface passivation and through the formation of hydroxyl radicals (•OH). In these experiments, birnessite surfaces remain pristine and do not sorb significant amounts of As(V); as a consequence, the overall As content in solution is constant despite all As(III) introduced in the system being oxidized to As(V) after 24 h under oxic conditions. In the perspective of water purification, a second processing step should thus aim at removing produced As(V) from solution, and the ability of two-line ferrihydrite (2L-Fh – Fig. S8) to sorb aqueous As(V) in the presence of PP was thus assessed owing to the strong affinity of As for Fe (oxyhdr)oxides (Dixit and Hering, 2003; Manning et al., 1998; Ona-Nguema et al., 2005; Raven et al., 1998; Redman et al., 2002). 2L-Fh was used for the As removal experiment to mimic conditions of water purification (Bhandari et al., 2011; Raven et al., 1998; Takaya et al., 2021). Interaction between a solution containing 0.5 mM As(V) and 2.5 mM PP, used as a typical product of the first processing step, with a 5 g/L 2L-Fh suspension allowed decreasing As(V) and PP concentration to vanishingly small values (Fig. S9a, b). Non-detectable concentrations of As(V) in solution are reached after 15 min in the presence of PP,

whereas in the absence of PP, due to the strong affinity of ferrihydrite for As(V), no As is detected in solution at the beginning of the experiment (Fig. S9a). In the former case, no aqueous phosphorous is detected either (Fig. S9b), most likely owing to the similar sorption behavior of As(V) and P(V) (Catarecha et al., 2007). Competitive sorption of arsenate and pyrophosphate anions to ferrihydrite is likely responsible for the observed delay in As(V) sorption in the presence of PP (Fig. S9a), but allows avoiding phosphorus release to the environment along water treatment. Meanwhile, no Fe is detected in solution (Fig. S9c), indicative of the absence of ferrihydrite dissolution along the process, despite the presence of PP.

4 Conclusion

Owing to the frequent coexistence of Fe(II) and As(III) species in groundwaters, the present study investigated the influence of the competitive oxidation of these two elements in the As(III)-MnO_2-PP-Fe(II) system. Relevance of the key positive influence of PP, a typical Mn(III) chelating agent, on As(III) oxidation by Mn oxides to these environmentally relevant systems was specifically investigated owing to the major implications in terms of treatment of such groundwaters. As reported previously, the presence of Fe(II) inhibits As(III) oxidation by birnessite in the absence of PP, owing to the precipitation of Fe (oxyhydr)oxides (lepidocrocite, ferrihydrite, and scorodite – $FeAsO_4$) at the birnessite surface, leading to its passivation. In the meantime, the formation of Fe (oxyhydr)oxides adsorbing a significant proportion of As(III) initially present in solution.

The addition of PP to the system significantly enhances As(III) oxidation by Mn oxides such as birnessite even in the presence of Fe(II) under circum-neutral pH conditions. This positive influence results both from the ability of PP to chelate Mn(III) and Fe(III), thus preventing birnessite surface passivation by Mn(III) and Fe(III) (oxyhydr)oxides, and from its role, when associated to Fe(II), in the formation of hydroxyl radicals (•OH) during the experiment. These radicals species are in turn able to oxidize further As(III). Finally, removal of As(V) through sorption to Fe (oxyhydr)oxides, the final step in the perspective of water treatment, is efficient even in the presence of significant concentrations of PP. Addition of Mn(III) chelating agents such as PP thus appears as an efficient way to enhance the oxidizing activity of

birnessite in large-scale treatment for arsenic detoxification of ground, drinking and waste waters.

Author contributions

C. Y. and X. F. designed the study. C. Y. and C. L. performed the experiments. C. Y. and L. Z. conducted X-ray absorption spectroscopy experiments. C. Y., F. Z., X. W., H. Y., W. T. and X. F. analyzed the data. B.L., C.Y., and X.F. led the overall discussion and manuscript writing. All co-authors discussed the results and commented on the manuscript. X. F. guided all aspects of the work.

Declaration of interest statement

The authors declare no competing interests.

Acknowledgments

This work was supported by National Natural Science Foundation of China (No. 42030709), the National Key Research and Development Program of China (No. 2017YFD0200201), and the program of China Scholarships Council (No. 202106760038). ISTerre is part of Labex OSUG@2020 (ANR10-LABX56).

Additional information

The online version contains supplementary material available including supplementary figures 1 to 9, and supplementary table 1.

Reference

Bhandari, N., Reeder, R.J. and Strongin, D.R. 2011. Photoinduced oxidation of arsenite to arsenate on ferrihydrite. Environ. Sci. Technol. 45(7), 2783-2789.

Camacho, L.M., Gutiérrez, M., Alarcón-Herrera, M.T., de Lourdes Villalba, M. and Deng, S. 2011. Occurrence and treatment of arsenic in groundwater and soil in northern Mexico and southwestern USA. Chemosphere 83(3), 211-225.

Catarecha, P., Segura, M.D., Franco-Zorrilla, J.M., García-Ponce, B., Lanza, M., Solano, R., Paz-Ares, J. and Leyva, A. 2007. A mutant of the Arabidopsis phosphate transporter PHT1; 1 displays enhanced arsenic accumulation. The Plant Cell 19(3), 1123-1133.

Cerkez, E.B., Bhandari, N., Reeder, R.J. and Strongin, D.R. 2015. Coupled redox transformation of chromate and arsenite on ferrihydrite. Environ. Sci. Technol. 49(5), 2858-2866.

Chen, Y., Graziano, J.H., Parvez, F., Liu, M., Slavkovich, V., Kalra, T., Argos, M., Islam, T., Ahmed, A., Rakibuz-Zaman, M., Hasan, R., Sarwar, G., Levy, D., van Geen, A. and Ahsan, H. 2011. Arsenic exposure from drinking water and mortality from cardiovascular disease in Bangladesh: prospective cohort study. BMJ 342, d2431.

Dixit, S. and Hering, J.G. 2003. Comparison of arsenic(V) and arsenic(III) sorption onto iron oxide minerals: implications for arsenic mobility. Environ. Sci. Technol. 37, 4182-4189.

Driehaus, W., Seith, R. and Jekel, M. 1995. Oxidation of arsenate(III) with manganese oxides in water treatment. Water Res. 29, 297-305.

Drits, V.A., Lanson, B. and Gaillot, A.C. 2007. Birnessite polytype systematics and identification by powder X-ray diffraction. Am. Mineral. 92(5-6), 771-788.

Ehlert, K., Mikutta, C. and Kretzschmar, R. 2014. Impact of birnessite on arsenic and iron speciation during microbial reduction of arsenic-bearing ferrihydrite. Environ. Sci. Technol. 48(19), 11320-11329.

Feng, X., Wang, P., Shi, Z., Kwon, K.D., Zhao, H., Yin, H., Lin, Z., Zhu, M., Liang, X., Liu, F. and Sparks, D.L. 2018. A quantitative model for the coupled kinetics of arsenic adsorption/desorption and oxidation on manganese oxides. Environ. Sci. Technol. Letter 5, 175−180.

Frisbie, S.H. and Mitchell, E.J. 2022. Arsenic in drinking water: An analysis of global drinking water regulations and recommendations for updates to protect public health. PLoS One 17(4), e0263505.

Gao, Z., Liu, J., Skurie, C., Zhu, Y. and Jun, Y.-S. 2022. Photochemical reactions of dissolved organic matter and bromide ions facilitate abiotic formation of manganese oxide solids. Water Res. 222, 118831.

Gude, J.C.J., Rietveld, L.C. and van Halem, D. 2017. As(III) oxidation by MnO_2 during groundwater treatment. Water Res. 111, 41-51.

Gunarathna, M., Kumari, M. and Nirmanee, K. 2016. Evaluation of interpolation methods for mapping pH of groundwater. International journal of latest technology in engineering, management & applied science 3, 1-5.

Gustafsson, J.P. and Antelo, J. 2022. Competitive arsenate and phosphate adsorption on ferrihydrite as described by the CD-MUSIC model. ACS Earth Space Chem. 6(5), 1397-1406.

Hájek, M., Jiménez-Alfaro, B., Hájek, O., Brancaleoni, L., Cantonati, M., Carbognani, M., Dedić, A., Dítě, D., Gerdol, R. and Hájková, P. 2020. A European map of groundwater pH and calcium. Earth System Science Data Discussions 2020, 1-41.

Han, X., Li, Y.-L. and Gu, J.-D. 2011. Oxidation of As(III) by MnO_2 in the absence and presence of Fe(II) under acidic conditions. Geochim. Cosmochim. Acta 75(2), 368-379.

He, Y.T. and Hering, J.G. 2009. Enhancement of arsenic(III) sequestration by manganese oxides in the presence of iron(II). Water, Air, Soil Pollut. 203, 359–368.

Herbel, M. and Fendorf, S. 2006. Biogeochemical processes controlling the speciation and transport of arsenic within iron coated sands. Chem. Geol. 228(1-3), 16-32.

Huang, J., Jones, A., Waite, T.D., Chen, Y., Huang, X., Rosso, K.M., Kappler, A., Mansor, M., Tratnyek, P.G. and Zhang, H. 2021. Fe(II) redox chemistry in the environment. Chem. Rev. 121(13), 8161-8233.

Huang, Y., Huangfu, X., Ma, C. and Liu, Z. 2023. Sequestration and oxidation of heavy metals mediated by Mn (II) oxidizing microorganisms in the aquatic environment. Chemosphere, 138594.

Jung, H., Chadha, T.S., Kim, D., Biswas, P. and Jun, Y.S. 2017. Photochemically assisted fast abiotic oxidation of manganese and formation of delta-MnO_2 nanosheets in nitrate solution. Chem. Commun. 53(32), 4445-4448.

Khachatryan, L. and Dellinger, B. 2011. Environmentally persistent free radicals (EPFRs)-2. Are free hydroxyl radicals generated in aqueous solutions? Environ. Sci. Technol. 45(21), 9232-9239.

Klewicki, J.K. and Morgan, J.J. 1999. Dissolution of β-MnOOH particles by ligands: Pyrophosphate, ethylenediaminetetraacetate, and citrate. Geochim. Cosmochim. Acta 63(19/20), 3017-3024.

Lafferty, B.J., Ginder-Voger, M. and Sparks, D.L. 2010. Arsenite oxidation by a poorly crystalline manganese-oxide 1. Stirred-flow experiments. Environ. Sci. Technol. 44(22), 8460-8466.

Lan, S., Wang, X., Xiang, Q., Yin, H., Tan, W., Qiu, G., Liu, F., Zhang, J. and Feng, X. 2017. Mechanisms of Mn(II) catalytic oxidation on ferrihydrite surfaces and the formation of manganese (oxyhydr)oxides. Geochim. Cosmochim. Acta 211, 79-96.

Lan, S., Ying, H., Wang, X., Liu, F., Tan, W., Huang, Q., Zhang, J. and Feng, X. 2018. Efficient catalytic As(III) oxidation on the surface of ferrihydrite in the presence of aqueous Mn(II). Water Res. 128, 92-101.

Lefkowitz, J.P., Rouff, A.A. and Elzinga, E.J. 2013. Influence of pH on the reductive transformation of birnessite by aqueous Mn(II). Environ. Sci. Technol. 47(18), 10364-10371.

Liang, M., Guo, H. and Xiu, W. 2020. Arsenite oxidation and arsenic adsorption on birnessite in the absence and the presence of citrate or EDTA. Environ. Sci. Pollut. Res.

Liao, S., Wang, X., Yin, H., Post, J.E., Yan, Y., Tan, W., Huang, Q., Liu, F. and Feng, X. 2020. Effects of Al substitution on local structure and morphology of lepidocrocite and its phosphate adsorption kinetics. Geochim. Cosmochim. Acta 276, 109-121.

Liu, W., Sun, B., Qiao, J. and Guan, X. 2019. Influence of pyrophosphate on the generation of soluble Mn(III) from reactions involving Mn oxides and Mn(VII). Environ. Sci. Technol. 53(17), 10227-10235.

Manning, B.A., Scott, F. and Goldberg, S. 1998. Surface structures and stability of arsenic(III) on goethite: spectroscopic evidence for inner-sphere complexes. Environ. Sci. Technol. 32, 2383-2388.

McKenzie, R.M. 1971. The synthesis of birnessite, cryptomelane, and some other oxides and hydroxides

of manganese. Miner. Mag. 38, 493-502.
Mikutta, C., Schröder, C. and Marc Michel, F. 2014. Total X-ray scattering, EXAFS, and Mössbauer spectroscopy analyses of amorphous ferric arsenate and amorphous ferric phosphate. Geochim. Cosmochim. Acta 140, 708-719.
Mock, R.P., Schaefer, M.V., Pacheco, J.L., Lake, L., Lee, I. and Ying, S.C. 2019. Influence of Fe(II) on arsenic(III) oxidation by birnessite in diffusion-limited systems. ACS Earth Space Chem. 3(4), 550-561.
Morgan, J.J., Schlautman, M.A. and Bilinski, H. 2021. Rates of abiotic Mn(II) oxidation by O_2: Influence of various multidentate ligands at high pH. Environ. Sci. Technol. 55(21), 14426-14435.
Morin, G. and Calas, G. 2006. Arsenic in soils, mine tailings, and former industrial sites. Elements 2(2), 97-101.
Nickson, R.T., McArthur, J.M., Ravenscroft, P., Burgess, W.G. and Ahmed, K.M. 2000. Mechanism of arsenic release to groundwater, Bangladesh and West Bengal. Appl. Geochem. 15, 403-413.
Nico, P.S. and Zasoski, R.J. 2001. Mn(III) center availability as a rate controlling factor in the oxidation of phenol and sulfide on δ-MnO_2. Environ. Sci. Technol. 35, 3338-3343.
Ona-Nguema, G., Morin, G., Juillot, F., Calas, G. and Brown, G.E. 2005. EXAFS analysis of arsenite adsorption onto two-line ferrihydrite, hematite, goethite, and lepidocrocite. Environ. Sci. Technol. 39(23), 9147-9155.
Oscarson, D.W., Huang, P.M., Defosse, C. and Herbillon, A. 1981. Oxidative power of Mn(IV) and Fe(III) oxides with respect to As(III) in terrestrial and aquatic environments. Nature 291, 50-51.
Pan, B., Sun, K. and Xing, B. 2010. Adsorption kinetics of 17α-ethinyl estradiol and bisphenol A on carbon nanomaterials. II. Concentration-dependence. J. Soils Sediments 10, 845-854.
Parikh, S.J., Lafferty, B.J., Meade, T.G. and Sparks, D.L. 2010. Evaluating environmental influences on As^{III} oxidation kinetics by a poorly crystalline Mn-oxide. Environ. Sci. Technol. 44, 3772–3778.
Podgorski, J. and Berg, M. 2020. Global threat of arsenic in groundwater. Science 368, 845–850.
Qian, A., Zhang, W., Shi, C., Pan, C., Giammar, D.E., Yuan, S., Zhang, H. and Wang, Z. 2019. Geochemical stability of dissolved Mn(III) in the presence of pyrophosphate as a model ligand: complexation and disproportionation. Environ. Sci. Technol. 53(10), 5768-5777.
Qin, W., Wang, Y., Fang, G., Liu, C., Sui, Y. and Zhou, D. 2016. Oxidation mechanism of As(III) in the presence of polyphenols: New insights into the reactive oxygen species. Chem. Eng. J. 285, 69–76.
Ravel, B. and Newville, M. 2005. ATHENA, ARTEMIS, HEPHAESTUS: Data analysis for X-ray absorption spectroscopy using IFEFFIT. J. Synchrotron Radiat. 12(4), 537-541.
Raven, K.P., Jain, A. and Loeppert, R.H. 1998. Arsenite and arsenate adsorption on ferrihydrite: kinetics, equilibrium, and adsorption envelopes. Environ. Sci. Technol. 32(3), 344-349.
Razo, L.M.D., García-Vargas, G.G., Valenzuela, O.L., Castellanos, E.H., Sánchez-Peña, L.C., Currier, J.M., Drobná, Z., Loomis, D. and Stýblo, M. 2011. Exposure to arsenic in drinking water is associated with increased prevalence of diabetes: a cross-sectional study in the Zimapán and Lagunera regions in Mexico. Environ. Health 10, 73.
Redman, A.D., Macalady, D.L. and Ahmann, D. 2002. Natural organic matter affects arsenic speciation and sorption onto hematite. Environ. Sci. Technol. 36, 2889-2896.
Schaefer, M.V., Plaganas, M., Abernathy, M.J., Aiken, M.L., Garniwan, A., Lee, I. and Ying, S.C. 2020.

615 Manganese, arsenic, and carbonate interactions in model oxic groundwater systems. Environ.
616 Sci. Technol. 54(17), 10621-10629.
617 Smith, A.H. and Steinmaus, C.M. 2011. Arsenic in drinking water. BMJ 342, d2248.
618 Spiro, T.G., Bargar, J.R., Sposito, G. and Tebo, B.M. 2010. Bacteriogenic manganese oxides. Acc. Chem.
619 Res. 43(1), 2-9.
620 Sun, B., Guan, X., Fang, J. and Tratnyek, P.G. 2015. Activation of manganese oxidants with bisulfite for
621 enhanced oxidation of organic contaminants: The involvement of Mn(III). Environ. Sci. Technol.
622 49(20), 12414-12421.
623 Sun, Q., Cui, P.-X., Fan, T.-T., Wu, S., Zhu, M., Alves, M.E., Zhou, D.-M. and Wang, Y.-J. 2018. Effects
624 of Fe(II) on Cd(II) immobilization by Mn(III)-rich δ-MnO_2. Chem. Eng. J. 353, 167–175.
625 Takaya, Y., Kadokura, M., Kato, T. and Tokoro, C. 2021. Removal mechanisms of arsenite by
626 coprecipitation with ferrihydrite. J. Environ. Chem. Eng. 9(5), 105819.
627 Trouwborst, R.E., Clement, B.G., Tebo, B.M., Glazer, B.T. and Luther, G.W., 3rd 2006. Soluble Mn(III)
628 in suboxic zones. Science 313(5795), 1955-1957.
629 Villalobos, M., Escobar-Quiroz, I.N. and Salazar-Camacho, C. 2014. The influence of particle size and
630 structure on the sorption and oxidation behavior of birnessite: I. Adsorption of As(V) and
631 oxidation of As(III). Geochim. Cosmochim. Acta 125, 564-581.
632 Wang, L., Wang, F., Li, P. and Zhang, L. 2013. Ferrous–tetrapolyphosphate complex induced dioxygen
633 activation for toxic organic pollutants degradation. Sep. Purif. Technol. 120, 148–155.
634 Wang, X., Li, X., Wang, L., Lanson, B., Zhu, M., Ying, C., Liang, X. and Feng, X. 2022. Effects of Mn
635 or Al incorporation on the structure, composition, and As (III) adsorption of oxidized green rust.
636 Chem. Geol. 611, 121124.
637 Wang, X., Wang, Q., Yang, P., Wang, X., Zhang, L., Feng, X., Zhu, M. and Wang, Z. 2020. Oxidation of
638 Mn(III) species by Pb(IV) oxide as a surrogate oxidant in aquatic systems. Environ. Sci. Technol.
639 54(21), 14124–14133.
640 Wang, Z., Xiong, W., Tebo, B.M. and Giammar, D.E. 2014. Oxidative UO2 dissolution induced by
641 soluble Mn(III). Environ. Sci. Technol. 48(1), 289-298.
642 Welch, K.D., Davis, T.Z. and Aust, S.D. 2002. Iron autoxidation and free radical generation: effects of
643 buffers, ligands, and chelators. Arch. Biochem. Biophys. 397(2), 360-369.
644 WHO 2011. Guidelines for drinking-water quality: Fourth Edition. WHO chronicle 38(4), 104-108.
645 Wu, Y., Kukkadapu, R.K., Livi, K.J.T., Xu, W., Li, W. and Sparks, D.L. 2018. Iron and arsenic speciation
646 during As(III) oxidation by manganese oxides in the presence of Fe(II): Molecular-level
647 characterization using XAFS, Mössbauer, and TEM analysis. ACS Earth Space Chem. 2(3),
648 256-268.
649 Wu, Y., Li, W. and Sparks, D.L. 2015. The effects of iron(II) on the kinetics of arsenic oxidation and
650 sorption on manganese oxides. J. Colloid Interface Sci. 457, 319-328.
651 Wu, Y., Li, Y., He, J., Fang, X., Hong, P., Nie, M., Yang, W., Xie, C., Wu, Z., Zhang, K., Kong, L. and
652 Liu, J. 2020. Nano-hybrids of needle-like MnO_2 on graphene oxide coupled with
653 peroxymonosulfate for enhanced degradation of norfloxacin: A comparative study and probable
654 degradation pathway. J. Colloid Interface Sci. 562, 1-11.
655 Ying, C., Lanson, B., Wang, C., Wang, X., Yin, H., Yan, Y., Tan, W., Liu, F. and Feng, X. 2020. Highly
656 enhanced oxidation of arsenite at the surface of birnessite in the presence of pyrophosphate and

the underlying reaction mechanisms. Water Res. 187, 116420.
Ying, S.C., Kocar, B.D. and Fendorf, S. 2012. Oxidation and competitive retention of arsenic between iron- and manganese oxides. Geochim. Cosmochim. Acta 96, 294–303.
Zhang, C., He, M., Ouyang, W., Lin, C. and Liu, X. 2020. Influence of Fe(II) on Sb(III) oxidation and adsorption by MnO_2 under acidic conditions. Sci. Total Environ. 724, 138209.
Zhang, F., Pan, Y., Ying, C., Wang, X., Yin, H., Tan, W., Wang, Z. and Feng, X. 2022. The effect of citric acid on the catalytic oxidation of Mn (II) on ferrihydrite surface. Appl. Geochem. 139, 105262.
Zhang, S., Chen, S., Liu, F., Li, J., Liang, X., Chu, S., Xiang, Q., Huang, C. and Yin, H. 2018. Effects of Mn average oxidation state on the oxidation behaviors of As(III) and Cr(III) by vernadite. Appl. Geochem. 94, 35-45.
Zhang, Y., Liu, X., Cheng, J. and Lu, X. 2021. Surface acidity and As(V) complexation of iron oxyhydroxides: Insights from first-principles molecular dynamics simulations. Environ. Sci. Technol. 55(23), 15921-15928.
Zheng, Q., Hou, J., Hartley, W., Ren, L., Wang, M., Tu, S. and Tan, W. 2020. As(III) adsorption on Fe-Mn binary oxides: Are Fe and Mn oxides synergistic or antagonistic for arsenic removal? Chem. Eng. J. 389, 124470.
Zhu, M., Paul, K.W., Kubicki, J.D. and Sparks, D.L. 2009. Quantum chemical study of arsenic(III, V) adsorption on Mn-oxides, implications for arsenic(III) oxidation. Environ. Sci. Technol. 43, 6655–6661.
Zhu, Y., Liang, X., Zhao, H., Yin, H., Liu, M., Liu, F. and Feng, X. 2017. Rapid determination of the Mn average oxidation state of Mn oxides with a novel two-step colorimetric method. Anal. Methods 9(1), 103-109.

Legends of figures and tables

Fig. 1 Evolution of As(III), As(V), and total As concentrations in solution during As(III) oxidation by birnessite in the presence of (a) 0 mM (Exp. Fe0.00_PP0.0), (b) 0.10 mM (Exp. Fe0.10_PP0.0), (c) 0.25 mM (Exp. Fe0.25_PP0.0), and (d) 0.50 mM Fe(II) (Exp. Fe0.50_PP0.0). (e) Relative proportion of initial As(III) occurring as As(III) and As(V) in solution after 24 h as a function of initial [Fe(II)] in the system. Evolution of (f) Fe and (g) Mn concentration in solution during As(III) oxidation by birnessite in the presence of 0, 0.10, 0.25, 0.50 mM Fe(II) (Exp. Fe0.00_PP0.0, Fe0.10_PP0.0, Fe0.25_PP0.0, and Fe0.50_PP0.0, respectively). Initial As(III) concentration: 0.5 mM, pH 7, 24 h.

Fig. 2 Evolution of As(III), As(V), and total As concentrations in solution during As(III) oxidation by birnessite in the presence of 0.50 mM Fe(II) and (a) 0.5 mM (Exp. Fe0.50_PP0.5), (b) 2.5 mM (Exp. Fe0.50_PP2.5), and (c) 5.0 mM PP (Exp. Fe0.50_PP5.0). (d) Relative proportion of initial As(III) occurring as As(III) and As(V) in solution after 24 h as a function of [PP] in the system. Evolution of (e) Fe and (f) total Mn and Mn(III) concentrations in solution during As(III) oxidation by birnessite in the presence of 0.50 mM Fe(II) and 0, 0.5, 2.5, 5.0 mM PP (Exp. Fe0.50_PP0.0, Fe0.50_PP0.5, Fe0.50_PP2.5, and Fe0.50_PP5.0, respectively). Initial As(III) concentration: 0.5 mM, pH 7, 24 h.

Fig. 3 FESEM micrographs of (a) initial birnessite, (b) solid products after As(III) oxidation by birnessite in the absence of PP (Exp. Fe0.0_PP0.0), (c) solid products after As(III) oxidation by birnessite in the presence of 0.5 mM Fe(II) (Exp. Fe0.50_PP0.0), and (d) solid products after As(III) oxidation by birnessite in the presence of 0.50 mM Fe(II) and 5.0 mM PP (Exp. Fe0.50_PP5.0). Initial As(III) concentration: 0.5 mM, pH 7, 24 h.

Fig. 4 (a) FTIR spectra of the initial birnessite (Bir) and of the solid reaction products of As(III) oxidation by birnessite (Exp. labels from Table 1). (b) As K-edge XANES spectra of the solid reaction products of As(III) oxidation by birnessite (Exp. Fe0.25_PP0.0 and Fe0.50_PP0.0 as solid red and yellow lines, respectively) and of reference As(III) and As(V) sorbed to ferrihydrite (dashed blue and green lines, respectively).

Fig. 5 As species ratios calculated from As speciation/concentration in aqueous and

712 solid fractions as a function of experimental conditions (Exp. labels from Table 1). (a)
713 As(III) and As(V) concentrations in solution are determined using LC-AFS, whereas
714 relative proportions of As(III) and As(V) in the solid reaction products are obtained
715 from LCF of As K-edge XANES spectra. As speciation in solid products was not
716 determined for Exp. Fe0.00_PP0.0 and Fe0.50_PP2.5. (b) Relative proportion of As in
717 the solid phase was obtained as the difference between aqueous As and initial As(III)
718 concentrations. Initial As(III) concentration: 0.5 mM, pH 7, 24 h.
719 **Fig. 6** Evolution as a function of reaction time of (a) As(III) and As(V), (b) Fe, and (c)
720 Mn concentrations in solution during As(III) oxidation by birnessite in the
721 absence/presence of PP and under anaerobic conditions (Exp. Fe0.50_PP0.0_Anox and
722 Fe0.50_PP5.0_Anox, respectively). Initial As(III) concentration: 0.5 mM, pH 7.
723 **Table 1** Experimental conditions used for As(III) oxidation
724

Supplementary data

Solutions for an efficient arsenite oxidation and removal from groundwater containing ferrous iron

Chaoyun Ying[a,b,c], *Chang Liu*[a,b], *Feng Zhang*[a,b], *Lirong Zheng*[d], *Xiaoming Wang*[a,b], *Hui Yin*[a,b], *Wenfeng Tan*[a,b], *Xionghan Feng*[a,b*], *Bruno Lanson*[c]

[a] State Environmental Protection Key Laboratory of Soil Health and Green Remediation, Wuhan 430070, China.

[b] Key Laboratory of Arable Land Conservation (Middle and Lower Reaches of Yangtze River), Ministry of Agriculture, College of Resources and Environment, Huazhong Agricultural University, Wuhan 430070, China.

[c] Univ. Grenoble Alpes, CNRS, Univ. Savoie Mont Blanc, IRD, Univ. Gustave Eiffel, ISTerre, F-38000 Grenoble, France.

[d] Beijing Synchrotron Radiation Facility, Institute of High Energy Physics, Chinese Academy of Sciences, Beijing 100039, China.

*Corresponding author:

Xionghan Feng,

Tel: +86 27 87280271; Fax: +86 27 87288618; E-mail: fxh73@mail.hzau.edu.cn

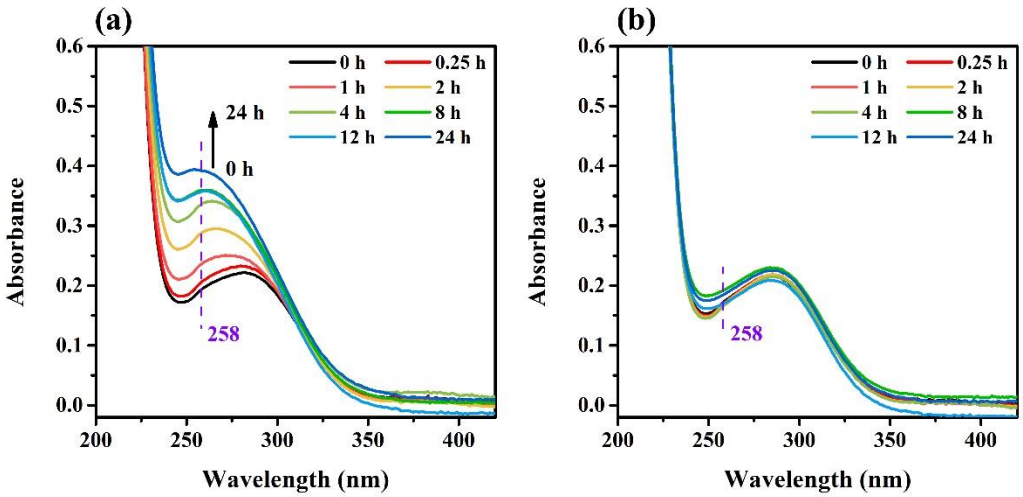

Fig. S1 (a) Evolution as a function of reaction time of solution UV-Vis absorption spectra during As(III) oxidation by birnessite in the presence of 0.50 mM Fe(II) and 2.5 mM PP (Exp. Fe0.50_PP2.5 after a 1:5 dilution in deionized water). (b) Evolution as a function of reaction time of As(III) solution UV-Vis absorption spectra in the presence of 0.50 mM Fe(II) and 2.5 mM PP (Exp. Fe0.50_PP2.5_NoBirn after a 1:5 dilution in deionized water). Initial As(III) concentration: 0.5 mM, pH 7.

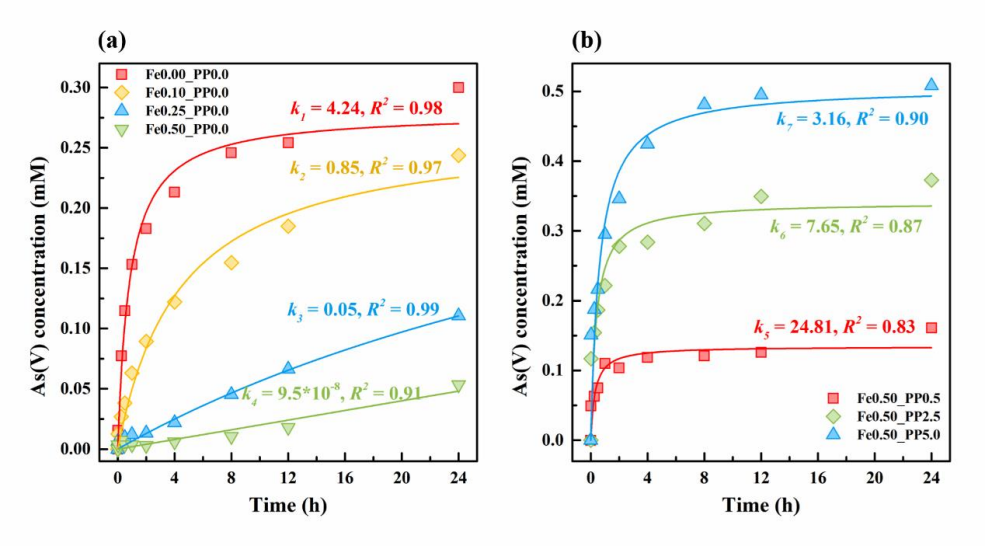

Fig. S2 Pseudo-second order modeling of As(V) formation kinetics during (a) As(III) oxidation by birnessite in the presence of 0 mM (Exp. Fe0.00_PP0.0), 0.10 mM (Exp. Fe0.10_PP0.0), 0.25 mM (Exp. Fe0.25_PP0.0), and 0.50 mM Fe(II) (Exp. Fe0.50_PP0.0) (b) As(III) oxidation by birnessite in the presence of 0.50 mM Fe(II) and 0.5 mM (Exp. Fe0.50_PP0.5), 2.5 mM (Exp. Fe0.50_PP2.5), and 5.0 mM PP (Exp. Fe0.50_PP5.0).

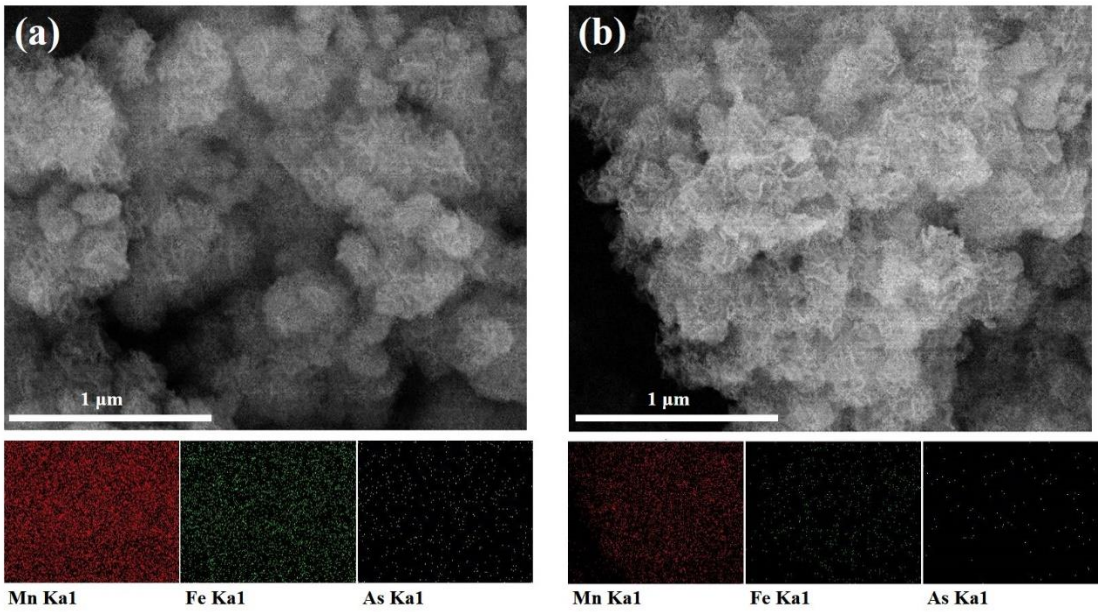

Fig. S3 FESEM micrographs and corresponding chemical maps (energy-dispersive X-ray fluorescence spectroscopy) of solid reaction products of As(III) oxidation by birnessite in the presence of (a) 0.5 mM Fe(II) and 0.0 mM PP and (b) 0.50 mM Fe(II) and 5.0 mM PP (Exp. Fe0.50_PP0.0 and Fe0.50_PP5.0, respectively). Initial As(III) concentration: 0.5 mM, pH 7, 24 h.

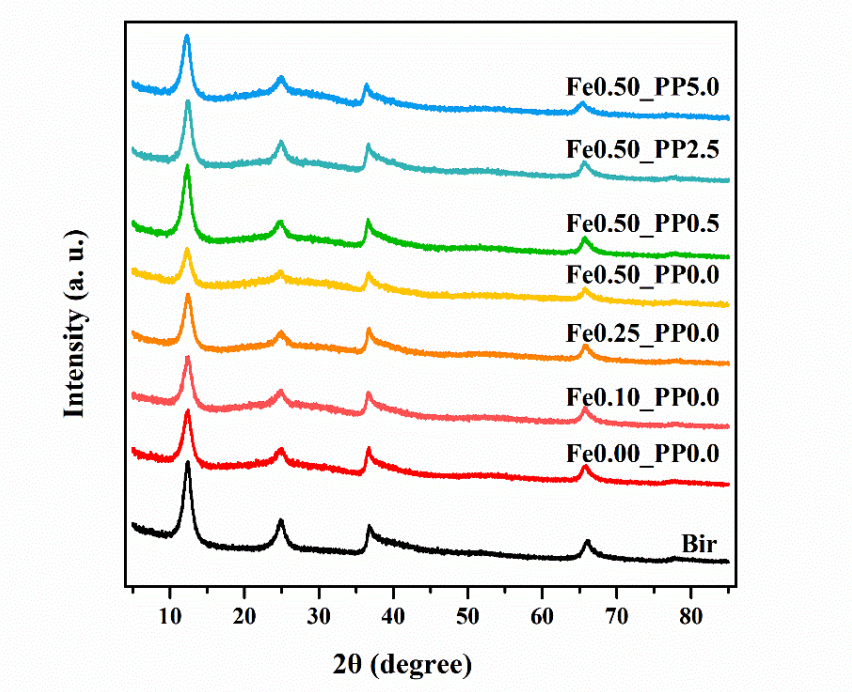

Fig. S4 X-ray diffraction patterns of initial birnessite (Bir), and of solid reaction products of As(III) oxidation by birnessite (Exp. labels from Table 1). Initial As(III) concentration: 0.5 mM, pH 7, 24h.

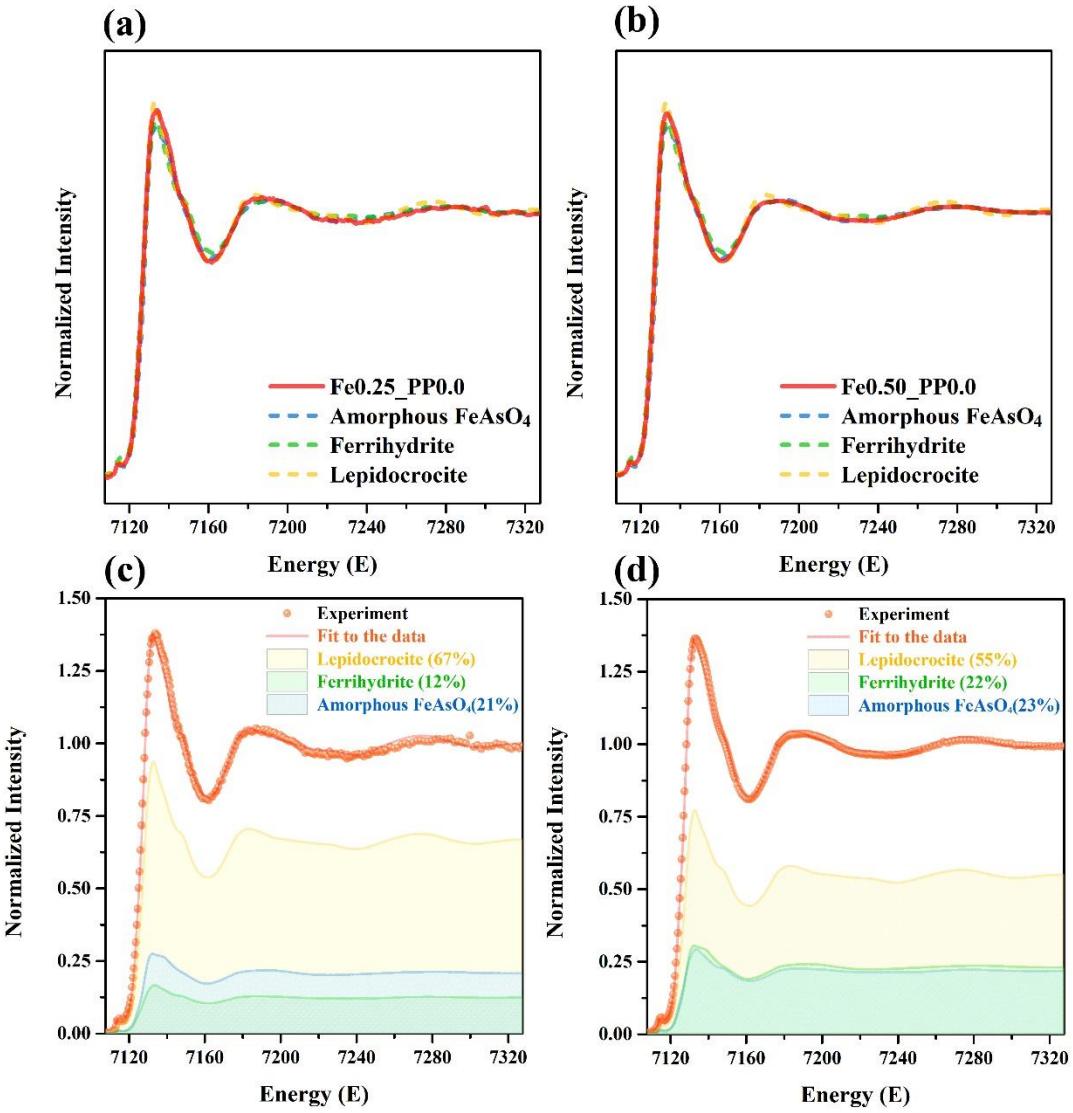

Fig. S5 Fe K-edge XANES spectra of the solid reaction products of As(III) oxidation by birnessite [(a) Exp. Fe0.25_PP0.0 (b) Exp. Fe0.50_PP0.0] superimposed with that of reference ferrihydrite, lepidocrocite, and amorphous scorodite. Linear combination fitting to the Fe K-edge XANES spectra of the solid reaction products of As(III) oxidation by birnessite [(c) Exp. Fe0.25_PP0.0 (d) Exp. Fe0.50_PP0.0] using ferrihydrite, lepidocrocite, and amorphous scorodite as references. Initial As(III) concentration: 0.5 mM, pH 7, 24 h.

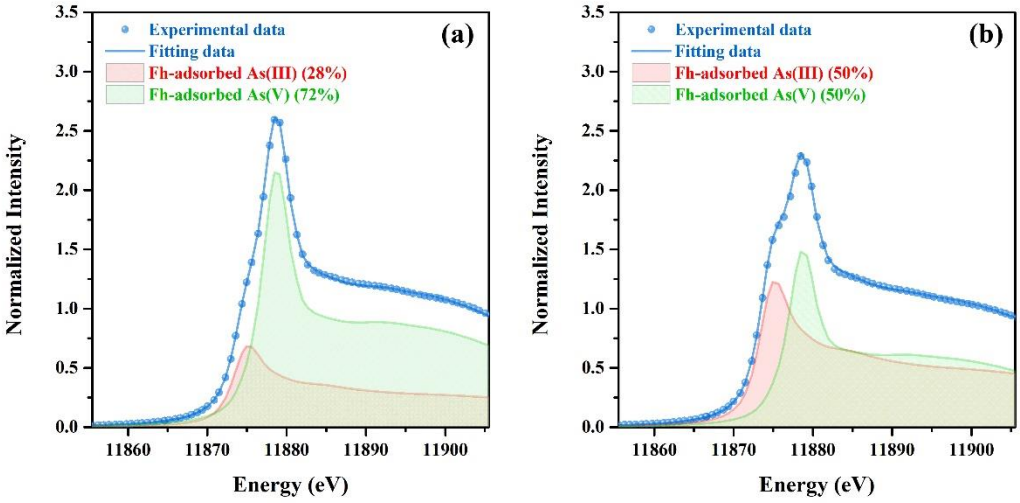

Fig. S6 Linear combination fitting to the As K-edge XANES of the solid reaction products of As(III) oxidation by birnessite (Exp. Fe0.25_PP0.0 and Fe0.50_PP0.0, left and right, respectively) using As(III)- and As(V)-sorbed ferrihydrite as references.

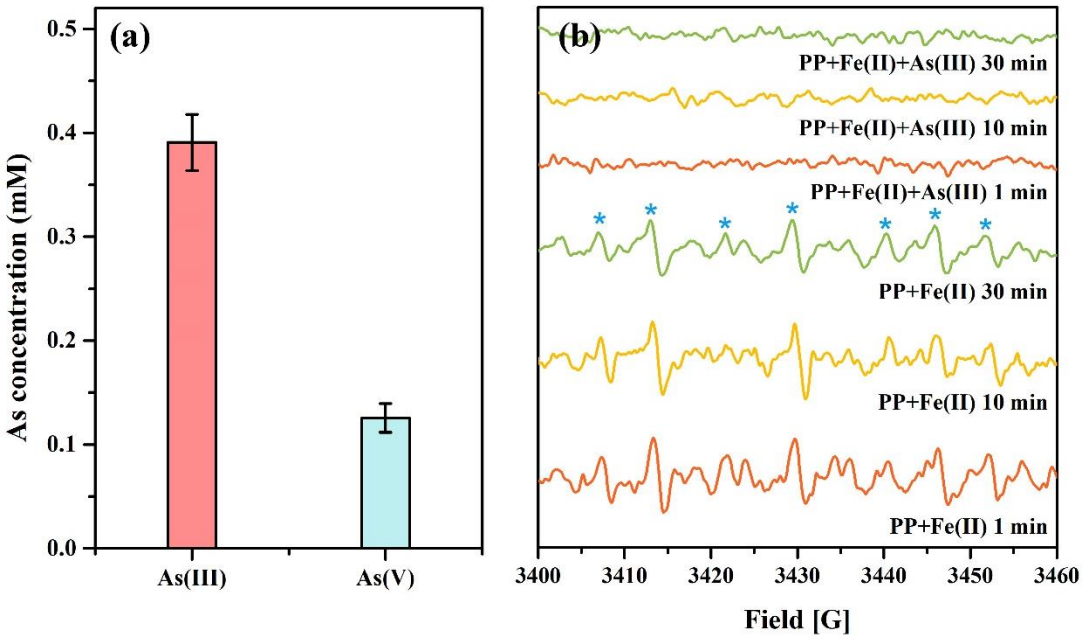

Fig. S7 (a) As(III) and As(V) concentrations in solution after As(III) oxidation in the absence of birnessite (Exp. Fe0.50_PP5.0_NoBirn). Initial As(III) concentration: 0.5 mM, pH 7, 24 h. (b) EPR spectra of solutions containing 0.5 mM Fe(II) and 5.0 mM PP (no birnessite) in the presence/absence of As(III) (Exp. Fe0.50_PP5.0_NoBirn and Fe0.50_PP5.0_NoBirnNoAs as shown green and red lines, respectively). pH 7; reaction times: 1, 10 and 30 min.

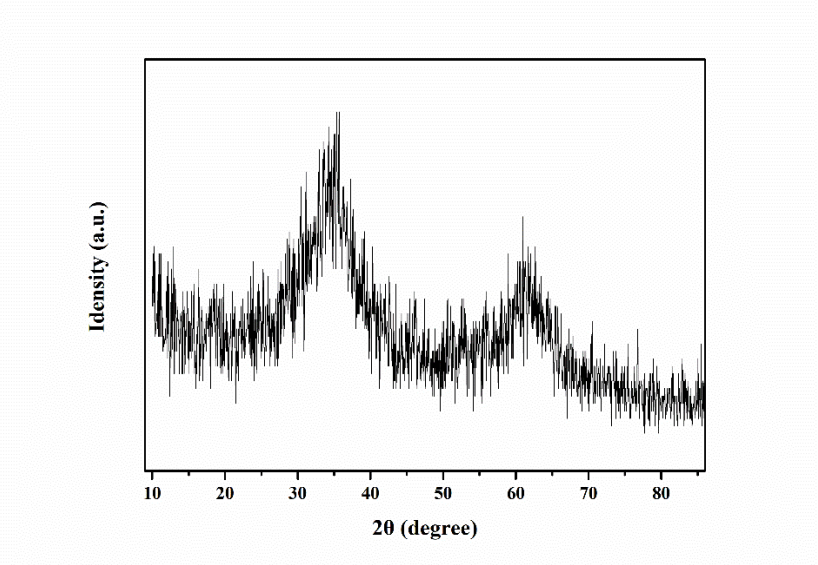

Fig. S8 X-ray diffraction pattern of synthetized two-line ferrihydrite (2L-Fh).

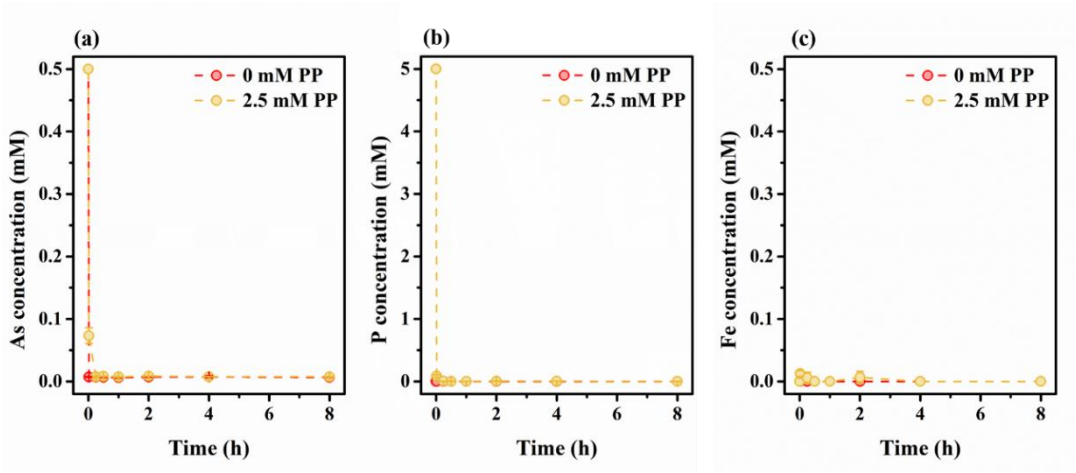

Fig. S9 Evolution as a function of reaction time of (a) As, (b) P, and (c) Fe concentrations in solution during As(V) adsorption to two-line ferrihydrite (2L-Fh) in the absence/presence of PP (0 and 2.5 mM PP concentrations shown with red and yellow patterns, respectively). Initial As(V) concentration: 0.5 mM, 5 g/L 2L-Fh, pH 7.

Table S1 Semi-quantitative chemical analysis (energy-dispersive X-ray fluorescence spectroscopy) of solid reaction products of As(III) oxidation by birnessite in the absence and presence of PP (Exp. Fe0.50_PP0.0 and Fe0.50_PP5.0, respectively). Initial As(III) concentration: 0.5 mM, pH 7, 24 h

	Elt.	Elt. Conc	Wt. %	At. %
Exp. Fe0.50_PP0.0	Mn K	86	78	81
	Fe K	11	10	10
	As L	8	12	9
Exp. Fe0.50_PP5.0	Mn K	22	100	100
	Fe K	0.00	0	0
	As L	0.00	0	0